AIMS Geosciences

AIMS Geosciences, 11(3): 790–805.
DOI: 10.3934/geosci.2025033
Received: 01 May 2025
Revised: 30 June 2025
Accepted: 14 August 2025
Published: 12 September 2025

https://www.aimspress.com/journal/geosciences

Research article

Effects of geomagnetic storms on cathodic protection systems in gas pipelines: A case study of disturbances in Argentina (2013-2018)

Patricia A Larocca and María A Arecco*

Universidad de Buenos Aires, Facultad de Ingeniería, Instituto de Geodesia y Geofísica Aplicadas, Ciudad Autónoma de Buenos Aires, Argentina

* **Correspondence:** Email: marecco@fi.uba.ar; Tel: +54-11-5285-0331.

Abstract: Gas pipelines are susceptible to telluric currents induced by temporal variations in the geomagnetic field (GMF), which are primarily driven by solar activity. These variations can generate electric fields at the Earth's surface, causing current flow through conductive infrastructure such as pipelines. In this study, we investigated the influence of GMF fluctuations on cathodic protection systems in gas pipelines, focusing on two major lines in Argentina: The NEUBA II (mid-latitude) and San Martín Fueguino (high-latitude) pipelines. Between 2013 and 2018, anomalies in Pipe-to-Soil Potential measurements were recorded at 38 monitoring points along these pipelines. We analyzed the relationship between PSP disturbances and geomagnetic and solar indices, including the Dst, Kp indices, Sunspot Number, and the F10.7 cm solar radio flux. In addition to global indices, we introduced the second vertical derivative (SVD) of the GMF as a method to detect rapid, localized magnetic field variations, even during geomagnetically quiet periods. Our findings revealed that such subtle GMF changes can produce Out-of-Range Protection Records, compromising cathodic protection systems, and potentially accelerating corrosion processes. We present an investigation into geomagnetic impacts on pipeline cathodic protection systems, with an application of SVD analysis. This research underscores the importance of integrating advanced geomagnetic monitoring tools into pipeline risk assessment and protection strategies. By correlating space weather parameters with ground-level effects, it provides a framework to better understand and mitigate geomagnetically induced currents, enhancing infrastructure resilience in both mid- and high-latitude regions. Our SVD results of the geomagnetic field are presented as a sensitive local indicator of disturbances affecting pipeline protection, especially under conditions where global geomagnetic indices suggest a quiet space weather.

Keywords: geomagnetic field; geomagnetic indices; solar indices; second vertical derivative; gas pipeline; pipeline soil potential; Argentina

1. Introduction

Geomagnetic field variations driven by solar activity can induce electric currents in long ground conductors, including pipelines [1–3]. While these effects have been widely documented in high-latitude regions and during strong geomagnetic storms, less attention has been given to the weak disturbances that can occur during geomagnetic quiet conditions, particularly in the mid- and high latitudes of the Southern Hemisphere. Here, we investigate the relationship between geomagnetic disturbances and pipeline cathodic protection system anomalies observed in Argentina between 2013 and 2018.

Gas pipelines are subject to the activity of telluric currents due to the temporal variation of the geomagnetic field (GMF), which results from solar activity. The changing GMF generates an electric field that causes charges to flow across the Earth's surface, which are then conducted through metallic networks located on it, such as pipelines, electrical transmission lines, and communication nets. This electrical disturbance is observed in pipelines as fluctuations in Pipe to Soil-Potential (PSP) and induced currents that can vary over time [4–7].

Variations in the GMF are associated with Earth's rotation, tidal cycles, the Sun's rotation, the eleven-year solar cycles, and solar storms [8,9]. The magnitude and location of these disturbances depend on the pipeline's proximity to the Earth's magnetic poles, its length, orientation, directional changes, coating resistance, electrical continuity along its route, soil resistivity, the presence of abrupt changes in soil conductivity, and proximity to a marine coast [1,10].

Various geomagnetic and solar indices are commonly used to characterize solar-terrestrial activity. Geomagnetic indices such as Dst and Kp reflect disturbances in geomagnetic field, while solar indices such as the Sunspot Number (SN) and the F10.7 solar radio flux represent solar activity levels.

The Disturbance Storm Time (Dst) index quantifies the intensity of geomagnetic storms by measuring variations in the GMF. It is derived by averaging the horizontal component of the magnetic field recorded at several low-latitude observatories near the geomagnetic equator.

However, the researchers in [11] argue that the Dst index is insufficient to fully characterize the presence and duration of a geomagnetic storm. In particular, storms driven by long-duration high-speed solar wind streams (commonly known as corotating interaction region or CIR-driven storms) may have weak and short-lived Dst signatures despite producing strong enhancements in radiation belt electron fluxes; one of the most significant space weather hazards [12,13].

The Kp index, introduced by Julius Bartels in 1949, measures geomagnetic activity by assessing the magnitude of solar particle radiation through its magnetic effects on the Earth. It has been in use since 1932 and remains a key parameter in space weather studies, providing insight into solar wind energy input and its effects on the upper atmosphere and climate variability. The index is derived from data collected at 13 geomagnetic observatories distributed around the globe.

The relative SN is another important index of solar activity, representing the total number of visible sunspots and sunspot groups on the solar disk. It is calculated daily, independent of previous observations. The official international sunspot number is provided by the Solar Influences Data Analysis Center (SIDC) at the Royal Observatory of Belgium.

The F10.7 index, which measures solar radio flux at a wavelength of 10.7 cm (2800 MHz), is a key proxy for solar activity. Originating from the solar chromosphere and corona, it closely correlates with sunspot numbers and solar extreme ultraviolet irradiance. This index has been recorded in Canada since 1947 making it one of the longest-running solar datasets. Unlike many solar indices, F10.7 can be reliably measured from Earth's surface in all weather conditions. Its values typically range from below 50 to over 300 solar flux units (s.f.u.) over a solar cycle. The data is provided by the National Research Council Canada in collaboration with Natural Resources Canada.

Historically, the effects of telluric currents on pipelines have been regarded as a minor inconvenience or curiosity in the context of cathodic protection studies aimed at meeting pipeline codes and regulatory standards [3,14]. However, with the increasing construction of pipelines at higher latitudes, in soils with higher resistivity, and using improved coating materials, disturbances in telluric potential have become more evident, particularly during intensified geomagnetic storms linked to heightened solar activity. Periods of peak solar activity have raised concerns about how to mitigate the influence of telluric currents and what techniques are available to accurately measure pipe-to-soil potentials during such geomagnetic events [2,15].

Although less pronounced, telluric effects have also been observed in pipelines located at lower latitudes, including near the equatorial region [6,16]. Notably, variations in PSP measurements were recorded between 2013 and 2018 along two major gas pipelines in Argentina: The NEUBA II pipeline, at mid-latitude, and the San Martín Fueguino pipeline, at high latitude. Detailed investigations revealed that these disturbances may be amplified by fluctuations in the GMF during geomagnetic storms [17,18]. Since the induced currents in these conductive structures discharge into the ground, producing fluctuations in potential, geomagnetic effects can be mitigated by identifying vulnerable segments and installing systems to safely discharge induced currents at specific locations. The design of such mitigation systems is fundamentally based on the ability to forecast geomagnetic activity [7].

While geomagnetic activity is primarily assessed using geomagnetic indices such as Dst and Kp, solar indices such as SSN and F10.7 provide the context in which geomagnetic disturbances could be triggered by solar events. These variations influence the PSP records and give rise to Out-of-Range Cathodic Protection Records (ORPR) at 38 monitoring points previously studied by [17,18] along the NEUBA II and San Martín Fueguino pipelines. The second vertical derivative (SVD) of the GMF was calculated, revealing correlations between rapid field variations and ORPR events.

One contribution of this work lies in the application of SVD to the geomagnetic field as a novel tool for detecting high-frequency local variations not captured by traditional global indices such as Dst or Kp. By correlating these disturbances with PSP records from two pipelines, we identify unexamined pipeline response patterns.

We overcame challenges due to the geographic and geomagnetic complexity of the pipeline locations, which range from mid-latitudes (NEUBA II pipeline in southwestern Buenos Aires Province) to high latitudes (San Martín Fueguino pipeline in northern Tierra del Fuego Province) (Figure 1). Buried pipelines traverse regions with markedly different soil types and conductivity characteristics, necessitating geophysical studies. Solar and geomagnetic indices were analyzed to assess their impact in these distinctive environments. While the solar indices (SSN and F10.7) have daily resolution and are not suitable for identifying short-term geomagnetic fluctuations, they were used in this study to assess the overall level of background solar activity during periods of PSP anomalies. The high values observed, even during geomagnetically quiet days, helped contextualize the possible external drivers of the geomagnetic field variability analyzed using the SVD.

Unlike researchers who have primarily focused on the effects of intense geomagnetic storms (e.g., [2,7]), we highlight scenarios where solar activity is elevated but geomagnetic indices remain relatively quiet.

2. Data sources and analytical methods for evaluating pipeline responses to geomagnetic activity

PSP records, provided by the gas transportation company, were analyzed to evaluate the performance of the cathodic protection system. Measurements were taken with the protection system both activated (PSP On) and deactivated (PSP Off), focusing on readings within the acceptable protection range (0.85 V to 1.35 V) and those falling outside this range, referred to as ORPR. PSP measurements were obtained using a $Cu/CuSO_4$ reference electrode installed at designated Control Points (CPs), specifically from CPs 650 to 790 along the NEUBA II pipeline, and from CPs 1 to 92 along the San Martín pipeline in Argentina.

For NEUBA II, data were analyzed over a 200 km segment near the locality of Goyena, located in the southwest of Buenos Aires (center Argentine). This section runs in a north-south direction and crosses the foothills of the Ventania mountain system. The pipeline traverses alluvial plain and terrace soils composed of unconsolidated Quaternary sediments, including silty clays, clayey silts, sandy materials, and sandy gravels with relatively thick, discontinuous layers of calcrete (tosca) of epigenic origin [19,20] (Figure 1a).

In the case of the San Martín pipeline, records were analyzed over a 100 km segment in Tierra del Fuego, southern Argentina. This section primarily lies on Mollisols; dark-colored, soft, and well-drained soils with high organic matter content [21]. The pipeline generally runs in a north-south direction, except for the final third, which turns west-east (Figure 1b).

Each pipeline segment includes between 100 and 200 control points, spaced approximately 1 to 1.5 kilometers apart. Both pipeline systems were studied over the period from 2013 to 2018.

To establish a correlation between ORPR and geomagnetic activity, records of the GMF were analyzed using data from the INTERMAGNET network (https://imag-data.bgs.ac.uk/GIN_V1/GINForms2). Data were obtained from the observatories closest to the pipeline control points (CPs) on the specific days when PSP measurements were taken. For the Goyena region, data from the Pilar Observatory (PIL, according to the International Association of Geomagnetism and Aeronomy—IAGA) were used, while for the Tierra del Fuego region, data from the Puerto Stanley/Puerto Argentino Observatory (PST) were utilized.

The Dst index is widely regarded as a reliable measure of the energy associated with geomagnetic storms [22]. It provides insight into whether the magnetosphere is experiencing quiet or disturbed conditions on a given day. The Dst index primarily reflects the strength of the ring current, a circulating flow of charged particles trapped by geomagnetic field. More negative Dst values correspond to stronger geomagnetic storms. Expressed in nanoteslas (nT), the Dst index is a widely used metric for assessing the severity of geomagnetic disturbances. A widely adopted classification based on minimum Dst values (cf. Table 1 in [23]) is as follows:

Weak storm: $-50\ \text{nT} < \text{Dst} \leqslant -30\ \text{nT}$

Moderate storm: $-100\ \text{nT} < \text{Dst} \leqslant -50\ \text{nT}$

Strong storm: $-200\ \text{nT} < \text{Dst} \leqslant -100\ \text{nT}$

Severe storm: $-350\ \text{nT} < \text{Dst} \leqslant -200\ \text{nT}$

Great storm: Dst < −350 nT

Dst index values were sourced from the Kyoto World Data Center (https://wdc.kugi.kyoto-u.ac.jp/dst_final/index.html).

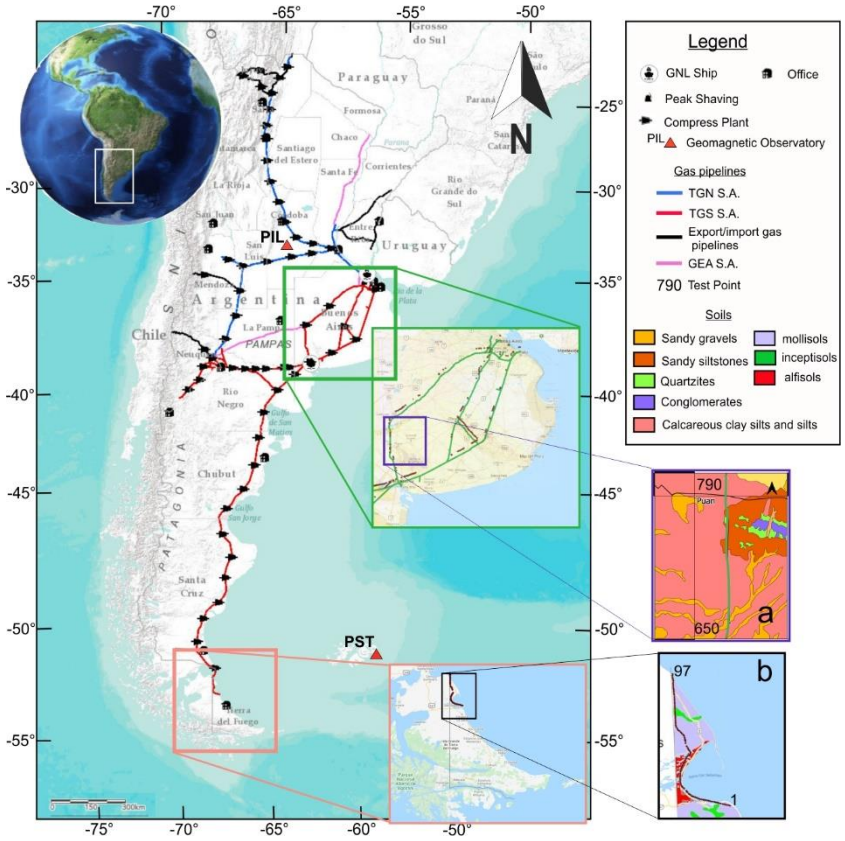

Figure 1. Map of pipelines and geomagnetic observatories. Pipelines in red, pink, black, and blue color; a) TGS S.A. pipeline location map Neuba II (red line) and control points (red stars) (source: https://www.enargas.gob.ar/secciones/informacion-geografica/diccionarios/diccionario.php#body). Green box: Section of Buenos Aires Province. Background image: Excerpt from the Geological and Mining Map of Buenos Aires Province (Source: SEGEMAR). Purple box: Details of the TGS gas pipeline. Background image: Coronel Suárez 3763-IV lithological map (Source: SEGEMAR). b) Location map of the TGS San Martín gas pipeline in Tierra del Fuego, Argentina (dotted pipe). Black box: Section of Tierra del Fuego Province. Background image from: https://arcg.is/01jSCn0.

In addition, tri-hourly values of the planetary Kp index were collected for each day on which ORPR events were observed to further characterize geomagnetic conditions (https://kp.gfz.de/en/). The geomagnetic indices Kp, and are produced by Geomagnetic Observatory Niemegk, GFZ German Research Centre for Geosciences. The values used here are described according to [24].

The international SN is given as the daily total sunspot number obtained from this source: http://www.sidc.be/silso/DATA/SN_d_tot_V2.0.txt, see http://www.sidc.be/silso/infosndtot.

Local noon-time observed (F10.7) solar radio flux F10.7 at 10.7 cm wavelength in s.f.u. (10^{-22} Wm^{-2} Hz^{-1}) is provided by Dominion Radio Astrophysical Observatory and Natural Resources Canada, see [25], see ftp://ftp.seismo.nrcan.gc.ca/spaceweather/solar_flux/daily_flux_values/fluxtable.txt.

A total of 2,053 PSP records were examined from both the NEUBA II and San Martín Fueguino gas pipelines over the period 2013–2018. These records included measurements taken with the cathodic protection system both active (PSP On) and inactive (PSP Off). Among them, 95 ORPRs were identified for the NEUBA II pipeline and 77 for the San Martín Fueguino pipeline.

Of these 172 ORPRs, 134 occurred during periods classified as mild or moderate geomagnetic storms, according to the criteria established by [23]. The remaining 38 ORPRs (18 from NEUBA II and 20 from San Martín) occurred on days without geomagnetic storms, as indicated by Dst index values greater than −5 nT.

To determine whether rapid variations in the GMF, even on geomagnetically quiet days, could be responsible for the occurrence of ORPRs, a detailed analysis of solar and geomagnetic indices was conducted. These included the Dst and Kp geomagnetic indices and the solar indices SN and the 10.7 cm solar radio flux (F10.7). Additionally, the SVD of the GMF was calculated to detect and assess short-term magnetic fluctuations. The SVD was performed because the first derivative study (dH/dt) was carried out on the NEUBA II gas pipeline. This application reinforces the results of the studies performed by the researchers in [17,18]

PSP measurements corresponding to ORPRs were recorded during several months across the study period: August, February, and November 2013; August 2014; January 2015; February, November, and December 2016; November 2017; and January 2018. For each of these instances, geomagnetic conditions were evaluated to determine whether they could explain the observed deviations, despite the presence of quiet solar activity (Dst > −5 nT).

The Kp index, which quantifies disturbances in the horizontal component of Earth's magnetic field, is derived from the maximum fluctuations observed in magnetometers at 13 observatories, mostly in the Northern Hemisphere, over three-hour intervals. Although considered a planetary index, it may not adequately reflect geomagnetic activity in the Southern Hemisphere. For this reason, the SVD of the GMF was calculated based on data from observatories in proximity to the study regions.

The SVD is a well-established method for enhancing weak or subtle features in geophysical signals, particularly in the absence of measurement noise. The SVD is typically computed, like any derivative, using the Fast Fourier Transform (FFT) [26] as well as a filter variable order vertical derivative [27]. This makes it particularly effective for identifying masked or low-amplitude signals.

To describe exactly and precisely the timing of rapid GMF fluctuations, derivatives were computed using the Fast Fourier Transform (FFT) in the frequency domain. The SVD was applied to total geomagnetic field (ϕ) data using the FFT VDRV program, which performs vertical derivative filtering on ϕ(t). The final computation of the SVD was performed according to equation (1).

$$\mathcal{F}\left[\frac{d^n\emptyset}{dt^n}\right] = (ik_t)^n\mathcal{F}[\phi] \tag{1}$$

where $\mathscr{F}$ is the Fourier transform, $\frac{d^n\emptyset}{dt^n}$ is the *nth-order derivative* of ϕ respect to *t* (time), ϕ is the GMF, *i* is the complex variable, *(ikt)* is the filter that transforms a function measured such as *n*th-order derivatives with respect to *t.* The SVD enhances variations in continuous functions by amplifying the high-frequency components, making it possible to pinpoint the precise moments when rapid fluctuations occur in the geomagnetic field, typically indicated by sharp peaks or local maxima. The SVD was calculated in Oasis montaj using FFT parameters set with a distance increment of 10 min and a linear interpolation method, creating a regularly spaced grid for analysis. Although the software

does not explicitly define a window size, the FFT is applied over the entire interpolated grid. The purpose of applying the SVD in this context is to detect sharp variations within spatial windows constrained to approximately 10 min.

3. Results

Figure 2 displays the monthly Dst index values corresponding to the periods when ORPRs were detected at Control Points (CPs). These Dst records reveal that the PSP measurements (On-Off) were taken during periods that do not qualify as geomagnetic storms based on the Dst index criteria. Nonetheless, the PSP values were anomalous, falling outside the cathodic protection range.

Table 1. PSP values measured in the NEUBA II gas pipeline, and solar and magnetic indices.

Test Point	Time (UTC)	PSP OFF (mV)	PSP ON (mV)	On-Off	ORPR (mV)	Dst (nT)	Kp	SN	F10.7 (s.f.u.)
782	26/8/2013 19:32	−0.925	−0.747	0.178	0.103	−4	1.667	43	111.2
781	26/8/2013 19:48	−0.946	−0.77	0.176	0.080	−4	1.667	43	111.2
780	26/8/2013 19:58	−0.912	−0.749	0.163	0.101	−4	1.667	43	111.2
779	26/8/2013 20:07	−0.907	−0.745	0.162	0.105	−4	1.667	43	111.2
778	26/8/2013 21:03	−0.995	−0.799	0.196	0.051	−5	1.667	43	111.2
777	26/8/2013 21:08	−0.961	−0.811	0.15	0.039	−5	1.667	43	111.2
776	26/8/2013 21:20	−0.977	−0.83	0.147	0.020	−5	1.667	43	111.2
774.2	26/8/2013 21:37	−0.969	−0.836	0.133	0.014	−5	1.667	43	111.2
712	19/8/2014 13:38	−1.631	−1.464	0.167	**0.114**	11	2.667	93	110.7
710	19/8/2014 15:00	−0.669	−0.512	0.157	**0.338**	10	1.667	93	110.7
709	19/8/2014 15:10	−0.97	−0.811	0.159	0.039	10	1.667	93	110.7
708	19/8/2014 15:15	−0.905	−0.745	0.16	**0.105**	10	1.667	93	110.7
707	19/8/2014 15:35	−0.689	−0.529	0.16	**0.321**	10	1.667	93	110.7
706	19/8/2014 16:01	−1.012	−0.844	0.168	0.006	12	2.667	93	110.7
702	19/8/2014 17:02	−1.02	−0.834	0.186	0.016	16	3.667	93	110.7
646	22/11/2016 11:48	−1.49	−1.489	0.001	**0.139**	11	2.333	0	77.3
794	3/12/2016 15:15	−0.852	−0.799	0.053	0.051	0	-	56	84.7
794	28/11/2017 21:50	−1.064	−0.844	0.22	0.006	3	-	15	71.9

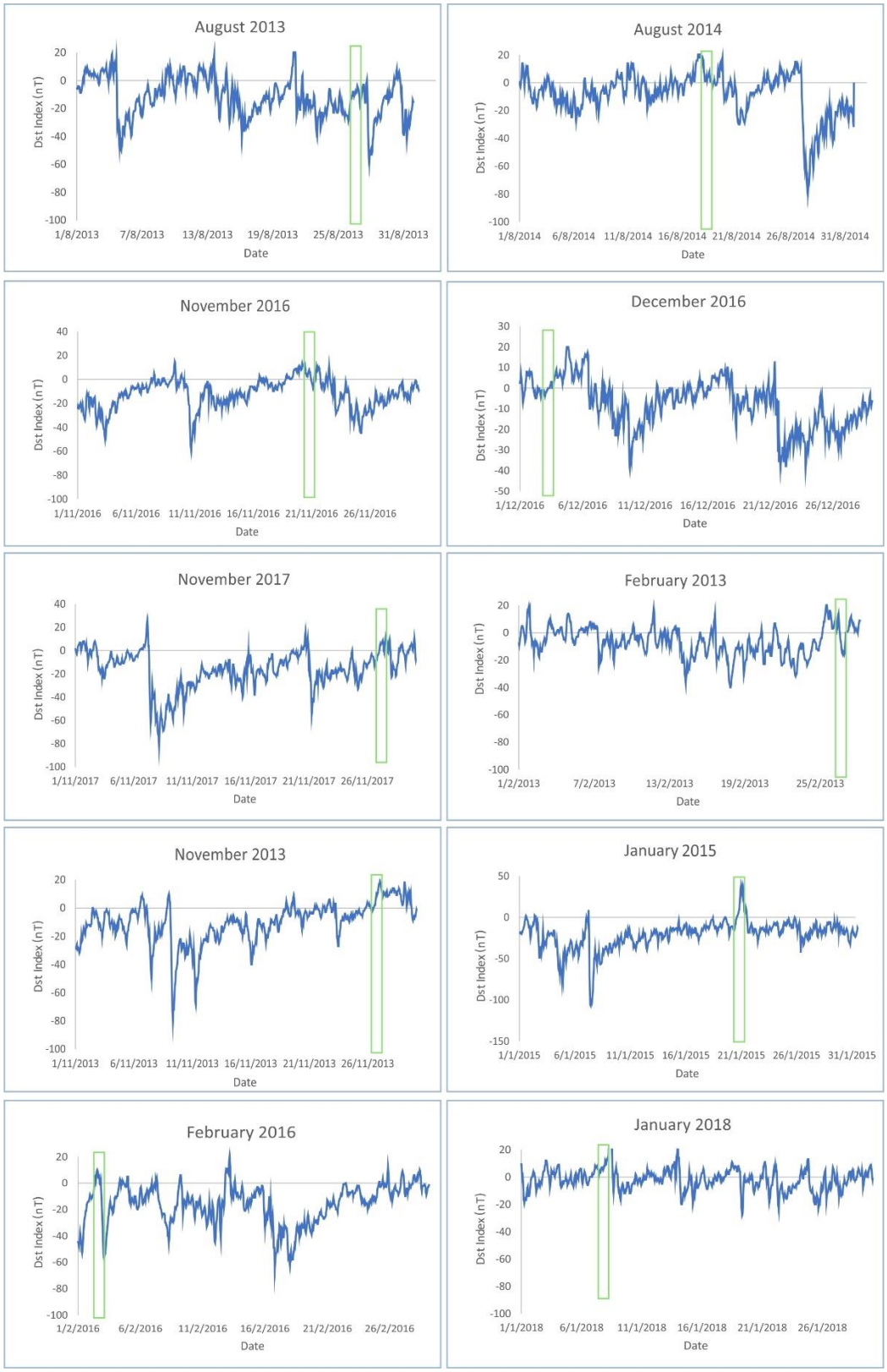

Figure 2. Dst hourly index in the months whose PSP were outside the cathodic protection range. August 2013, August 2014, November 2016, December 2016, and November 2017 in the NEUBA II pipeline. February 2013, November 2013, January 2015, February 2016, and January 2018 in the San Martín pipeline. The green box indicates the measurement interval.

Table 2. PSP values measured in the San Martín gas pipeline, and solar and magnetic indices.

Test Point	Time (UTC)	PSP OFF (mV)	PSP ON (mV)	On-Off	ORPR (mV)	Dst (nT)	Kp	SN	F10.7 (s.f.u.)
81.811	27/2/2013 12:22	−1.040	−0.809	0.231	0.041	12	0.667	58	100
70	27/2/2013 20:34	−1.010	−0.800	0.210	0.050	2	0	58	100
17.632	27/11/2013 15:35	−1.056	−0.807	0.249	0.043	11	0.667	73	129
97.2	21/1/2015 11:34	−1.510	−0.790	0.720	0.060	19	1.667	43	123.9
89	21/1/2015 16:03	−1.040	−0.794	0.246	0.056	4	2	43	123.9
65.8	2/2/2016 13:46	−1.02	−0.781	0.239	**0.069**	9	1.333	52	102.1
66	2/2/2016 14:28	−1.033	−0.791	0.242	0.059	10	1.333	52	102.1
71	2/2/2016 14:49	−0.971	−0.784	0.187	0.066	9	1.333	52	102.1
76	2/2/2016 15:16	−0.956	−0.785	0.171	0.065	9	1.333	52	102.1
77	2/2/2016 15:45	−1.001	−0.793	0.208	0.057	4	1.333	52	102.1
78	2/2/2016 16:10	−0.965	−0.782	0.183	**0.068**	4	1.333	52	102.1
82	2/2/2016 16:50	−0.986	−0.783	0.203	**0.067**	4	1.333	52	102.1
83	2/2/2016 17:01	−1.017	−0.796	0.221	0.054	4	1.333	52	102.1
84	2/2/2016 17:20	−1.009	−0.785	0.224	0.065	4	1.333	52	102.1
85	2/2/2016 17:37	−1.011	−0.773	0.238	**0.077**	5	1.333	52	102.1
87	2/2/2016 17:54	−1.045	−0.794	0.251	0.056	−1	2	52	102.1
95	2/2/2016 20:39	−1.057	−0.794	0.263	0.056	1	2	52	102.1
97.2	2/2/2016 21:11	−2.19	−0.794	1.396	0.056	1	2	52	102.1
1	10/1/2018 16:32	−1.650	−0.800	0.850	0.050	−3	1	20	70.4
2	10/1/2018 17:13	−1.600	−0.800	0.800	0.050	−5	1	20	70.4

Table 3. Date and time of acquisition of PSP OFF and PSP ON on test points for both gas pipelines. Calculation of ON-OFF and CPR. Values of solar and geomagnetic indices.

Test Point	Time (UTC)	PSP OFF (mV)	PSP ON (mV)	On-Off	CPR (mV)	Dst (nT)	Kp	SN	F10.7 (s.f.u.)
799	26/8/2013 11:18	−1.168	−0.863	0.305	0.013	−8	1.000	43	111.2
704	19/8/2014 14:00	−1.039	−0.878	0.161	0.028	11	1.667	93	110.7
613	22/11/2016 07:00	−1.42	−1.080	0.340	0.230	1	1.000	0	75.4
795	3/12/2016 14:41	−0.995	−0.936	0.059	0.086	7	0.000	56	82.2
773	28/11/2017 09:24	−1.304	−0.996	0.380	0.146	−16	1.667	15	71.9
77	27/2/2013 14:01	−1.081	−0.865	0.216	0.015	9	1.333	58	102.0
60	27/11/2013 10:50	−1.426	−1.039	0.387	0.189	9	0.000	73	125.6
44	21/1/2015 09:10	−1.304	−1.12	0.184	1.970	7	1.667	43	123.9
52	2/2/2016 09:38	−1.371	−1.174	0.197	0.324	3	0.667	53	102.1
61	10/1/2018 10:42	−1.435	−1.009	0.426	0.159	−4	1.000	20	68.1

Within each green box in Figure 2, the Dst index fluctuates from positive to slightly negative values, ranging between +50 nT and −10 nT. This range does not indicate the presence of a geomagnetic storm. Consequently, these specific PSP records were selected for further analysis in

relation to other geomagnetic activity indicators that may detect disturbances not captured by the Dst index, such as the Kp index, the SN, and the F10.7 solar flux index (Tables 1 and 2).

Additionally, PSP records within the acceptable cathodic protection range were included from the same dates to enable comparison with the anomalous values (Table 3).

Regarding the SN, the measurement period coincides with the declining phase of Solar Cycle 24, whose peak activity reached 113 sunspots in June 2014. The annual average sunspot numbers for the measurement period were: 94.0 in 2013, 113.3 in 2014, 69.8 in 2015, 39.8 in 2016, 21.7 in 2017, and 7.0 in 2018. On the specific PSP measurement dates, sunspot numbers were relatively high compared to the annual averages (Tables 1 and 2).

The F10.7 solar radio flux index, which typically ranges from 50 to 300 solar flux units (sfu), showed moderate values on the selected days, suggesting disturbances in the average solar wind (Tables 1 and 2).

The Kp geomagnetic index, which ranges from 0 (quiet) to 9 (severe geomagnetic activity), remained below 3 on all selected days, indicating geomagnetically quiet conditions (Tables 1 and 2).

The GMF measurements from the Pilar (PIL) and Puerto Stanley/Puerto Argentino (PST) observatories during the ORPR dates showed minimal disturbances (Figure 3a). To detect minor variations in the GMF, the SVD was applied. The resulting SVD curves exhibited high-frequency oscillations and intermittent peaks with amplitudes ranging from ± 4 to ± 40 × 10^{-6} nT·m^{-2}. Notably, the timing of these peaks corresponded closely with PSP records that fell outside the cathodic protection range, despite the days being classified as geomagnetically quiet (Figure 3a).

Table 4. Comparison of the range of the Second Vertical Derivative (SVD) recorded on selected days with that reached during the geomagnetic superstorm of May 11, 2024.

Date	SVD Range (nT·m^{-2})	SVD Maximum (nT·m^{-2})	% SVD Maximum rate
August 26, 2013	(−4 and 4) × 10^{-6}	5.7 × 10^{-6}	3
August 19, 2014	(−20 and 40) × 10^{-6}	43 × 10^{-6}	23
November 22, 2016	(−10 and 20) × 10^{-6}	21.0 × 10^{-6}	11
December 3, 2016	(−10 and 20) × 10^{-6}	20,5 × 10^{-6}	11
November 28, 2017	(−10 and 20) × 10^{-6}	18,5 × 10^{-6}	10
February 27, 2013	(−8 and 8) × 10^{-6}	8.1 × 10^{-6}	4
November 27, 2013	(−10 and 10) × 10^{-6}	14.1 × 10^{-6}	8
January 21, 2015	(−20 and 40) × 10^{-6}	51.7 × 10^{-6}	28
February 2, 2016	(−10 and 10) × 10^{-6}	0.9 × 10^{-6}	1
January 10, 2018	(−20 and 30) × 10^{-6}	16.2 × 10^{-6}	9
May 11, 2024	(−200 and 200) × 10^{-6}	187,8 × 10^{-6}	100

In Figure 3a, red rectangles indicate time intervals when PSP values fell outside the protection range, while green rectangles mark periods when the PSP remained within acceptable cathodic protection limits. The SVD line shows distinct amplitude peaks during the same intervals in which PSP records deviated from the protective range, specifically on the following dates: August 19, 2014; November 22, 2016; December 3, 2016; November 28, 2017; February 27, 2013; January 21, 2015; February 2, 2016; and January 10, 2018.

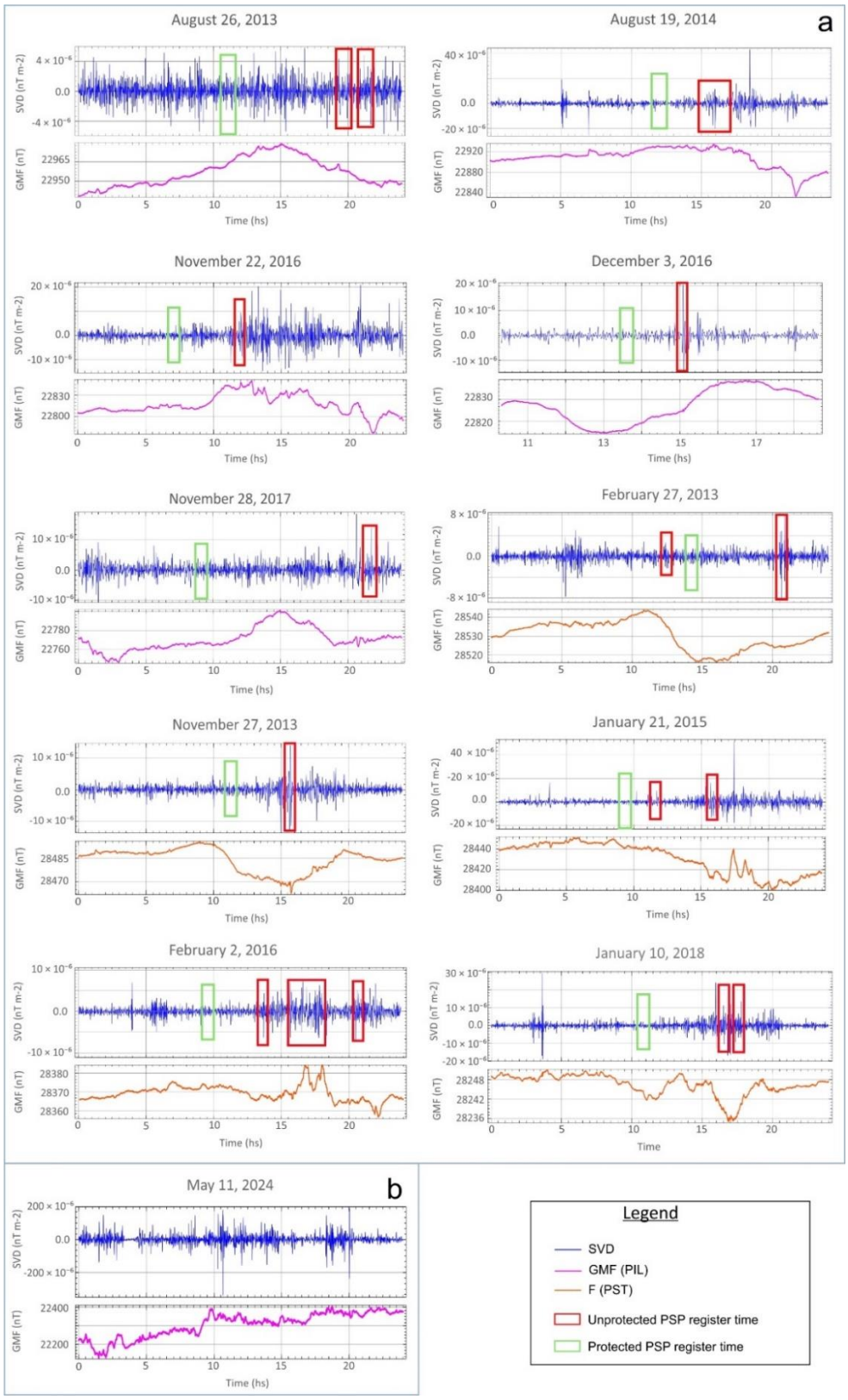

Figure 3. a. Geomagnetic field (GMF) modulus of the selected days in ORPR state taken at the observatories closest to the Test Points: PIL (pink line) and PST (orange line). Second vertical derivative (SVD) (blue line). SVD values at the PSP measurement time (green box). b. GMF (pink line) and SVD (blue line). Enclosed in the red boxes are the SVD peaks associated with the ORPR (Tables 1 and 2).

To further evaluate the significance of these SVD peaks and compare their magnitudes with those observed during a known high-activity event, the May 11, 2024 geomagnetic superstorm, the maximum SVD amplitudes recorded on ORPR days were compared with those recorded during the storm (Figure 3b). While the SVD amplitudes on the selected quiet days reached up to $\pm$ 40 $\times$ 10^{-6} nT·m^{-2}, the superstorm exhibited peaks up to $\pm$ 200 $\times$ 10^{-6} nT·m^{-2} —an order of magnitude higher (Table 4).

4. Discussion

In the context of our observations, it is important to highlight that certain geomagnetic disturbances may remain unclassified under traditional Dst-based criteria, despite their capacity to significantly heat the ion plasma sheet. During such events, hot ions predominantly drift tangentially and fail to penetrate the inner magnetosphere, leading to a weak ring current and, consequently, a minimal response in the Dst index. This phenomenon likely contributed to the apparent discrepancy between the elevated solar activity and the classification of geomagnetic conditions as quiet. Indeed, although all measurements were recorded during periods deemed geomagnetically quiet according to both Dst and Kp indices, solar indicators such as the SN and the solar radio flux index (F10.7) revealed otherwise. Specifically, SN values ranged from 52 to 93, while F10.7 exhibited average values between 102.1 and 123.9 s.f.u. These elevated indices suggest that significant solar activity was present throughout the study period, underscoring the limitations of relying solely on global geomagnetic indices to characterize the space weather conditions relevant to ground-based technological systems such as buried pipelines.

The SVD analysis of the GMF provides further knowledge. On days when ORPRs were detected, the SVD revealed perturbations in the GMF with amplitudes exceeding 10% relative to the rest of the day (Figure 3), suggesting that geomagnetic variability may influence pipeline protection even during non-storm conditions. SVD enhances the detection of localized magnetic field anomalies by attenuating regional-scale variations, making it particularly useful for identifying subtle, high-frequency perturbations in geomagnetically quiet periods. These perturbations may not be captured by global indices like Dst or Kp but can significantly impact induced currents in long conductive systems such as pipelines. The SVD thus serves as a more sensitive diagnostic for potential cathodic protection disruptions.

Regarding soil conductivity along the gas pipeline routes, a wide range of electrical conductivities was observed. Field campaigns conducted by the Argentine Geological and Mining Service (SEGEMAR) have shown that the NEUBA II pipeline traverses a lowland plain where groundwater flow continuity increases toward discharge areas [19]. However, at the Control Points (CPs) where notable PSP voltage variations were recorded, the soil conductivity remained relatively uniform (Figure 1a).

Our findings demonstrate that PSP anomalies occurred even during geomagnetically quiet periods, as defined by Dst values greater than −30 nT and Kp values below 3. This challenges the adequacy of global indices alone in assessing GIC-related risks. In particular, SVD analysis revealed high-frequency perturbations that temporally coincided with ORPRs, confirming its usefulness as a complementary indicator.

Moreover, when comparing the two pipelines, we observed that the San Martín pipeline, at a higher geomagnetic latitude, exhibited a greater number of ORPR events. This is consistent with prior knowledge that GIC intensity increases with geomagnetic latitude due to the higher exposure to ionospheric currents. However, we also found that local soil conductivity influenced the PSP response.

Low-conductivity soils in Tierra del Fuego appeared to amplify the voltage disturbances. These results agree with the mechanisms proposed by [1,2, 28–30] but our study provides quantitative evidence from South American sites, which are underrepresented in the literature.

In summary, the combination of SVD-based detection, geographic factors, and soil electrical properties provides a more complete picture of geomagnetic impacts on pipeline systems, particularly under non-storm conditions.

In contrast, soils along the San Martín pipeline are predominantly well-drained and do not favor significant salt accumulation in any horizon, resulting in low electrical conductivity values ranging from 0.30 to 0.90 $dS \cdot m^{-1}$ [31]. The study region experiences annual precipitation between 300 and 430 mm, distributed fairly evenly throughout the year [32]. Although, rainfall decreases significantly between November and February (below 100 mm), creating a seasonal pattern. Combined with the region's gently undulating topography, this promotes the formation of wetter zones with localized water accumulation, potentially increasing soil conductivity in those areas. Despite this, the mineralogical composition of the parent material and its limited weathering result in generally low soil conductivity across the region, with values ranging from 0.01 to 0.36 $dS \cdot m^{-1}$ (Figure 1b).

5. Conclusions

Although the pipelines are at different magnetic latitudes, NEUBA II in lower magnetic latitudes and San Martín in higher ones, both exhibited instances of cathodic protection failure, even on days without recorded geomagnetic disturbances.

These findings suggest that elevated solar activity, as indicated by high SN and F10.7 solar flux values, can influence the Earth's electromagnetic environment even under geomagnetically quiet conditions, as classified by the Dst and Kp indices. Therefore, these solar indicators may play a significant role in assessing potential failures in cathodic protection systems, given their association with solar radiation and charged particle fluxes that can induce geomagnetically induced currents (GICs) in pipelines.

The results support the conclusion that the SVD of the GMF is a sensitive indicator of high-frequency local perturbations that are not necessarily captured by global indices such as Dst. The maximum amplitude peaks identified in the SVD correspond to abrupt variations in the GMF, which can adversely impact the effectiveness of cathodic protection systems. This is evidenced by PSP measurements falling outside the protection threshold, even on days classified as geomagnetically quiet based on Dst values.

The analysis of soil conductivity along the NEUBA II and San Martín gas pipelines reveals distinct geoelectrical environments. These findings suggest that PSP anomalies are not solely attributable to soil conductivity, indicating a stronger influence of geomagnetic factors or structural conditions on the pipelines.

These observations underscore the importance of long-term monitoring of PSP variations to build a reliable statistical database on the frequency and magnitude of extreme fluctuations. Such data is crucial for assessing the risk of corrosion driven by telluric currents and for validating statistical prediction models aimed at mitigating the effects of space weather on pipeline infrastructure.

We introduce the use of the SVD as an effective method for detecting rapid and localized geomagnetic variations not captured by traditional indices such as Dst or Kp. Our findings demonstrate that observations from local geomagnetic observatories enhance the information provided by global

indicators, improving the results by providing detailed in-situ monitoring of the phenomenon. This knowledge is crucial for developing more accurate models and mitigation strategies for buried pipeline infrastructure, particularly in understudied regions of the Southern Hemisphere.

Author contributions

Conceptualization: P. Larocca and M. Arecco; Ressources: P. Larocca and M. Arecco; Data curation: P. Larocca and M. Arecco; Formal analysis: P. Larocca and M. Arecco; Supervision: P. Larocca; Validation: P. Larocca; Investigation: P. Larocca and M. Arecco; Writing —original draft: P. Larocca and M. Arecco; Methodology: M. Arecco; Project administration: M. Arecco; Writing—review & editing: P. Larocca and M. Arecco. All authors have read and agreed to the published version of the manuscript.

Use of AI tools declaration

The authors declare they have not used Artificial Intelligence (AI) tools in the creation of this article.

Acknowledgments

This work was partially supported by research projects from the Universidad de Buenos Aires.

Conflict of Interest

The authors declare that they have no known competing financial interests or personal relationships that could have appeared to influence the work reported in this paper.

References

1. Boteler D (2013) A new versatile method for modelling geomagnetic induction in pipelines. *Geophys J Int* 193: 98–109. https://doi.org/10.1093/gji/ggs113
2. Ingham M, Rodger CJ (2018) Telluric Field Variations as Drivers of Variations in Cathodic Protection Potential on a Natural Gas Pipeline in New Zealand. *Space Weather* 16: 1396–1409. https://doi.org/10.1029/2018SW001985
3. Hejda P, Bochniek J (2005) Geomagnetically induced pipe to soil voltages in the Czech oil pipelines during October-November 2003. *Ann Geophys* 23: 3089–3093. https://doi.org/10.5194/angeo-23-3089-2005
4. Trichtchenko L, Boteler DH (2001) Specification of geomagnetically induced electric fields and currents in pipelines. *J Geophys Res: Space Phys* 106: 21039–21048. https://doi.org/10.1029/2000JA000207
5. Fernberg PA, Samson C, Boteler DH, et al. (2007) Earth conductivity structures and their effects on geomagnetic induction in pipelines. *Ann Geophys* 25: 207–218. https://doi.org/10.5194/angeo-25-207-2007

6. Marshall RA, Waters CL, Sciffer MD (2010) Spectral analysis of pipe-to-soil potentials with variations of the Earth's magnetic field in the Australian region. *Space Weather* 8. https://doi.org/10.1029/2009SW000553
7. Trichtchenko L, Trishchenko AP, Hejda P, et al. (2023) Evaluation of telluric-associated corrosion on buried pipelines. *J Atmos Sol-Terr Phys* 248: 106082. https://doi.org/10.1016/j.jastp.2023.106082
8. Dobrică V, Demetrescu C (2024) The geomagnetic field and the earth's rotation. Connection at sub-centennial and inter-decadal timescales. *Rev Roum Géophysique* 67: 35–42. https://doi.org/10.59277/rrgeo.2024.67.5
9. Dwivedi D, Chandrasekhar NP (2024) Geomagnetic field variations due to solar tides at the Indian Observatories. *Earth Planets Space* 76: 61. https://doi.org/10.1186/s40623-024-01996-8
10. Osella A, Favetto A (2000) Effects of soil resistivity on currents induced on pipelines. *J Appl Geophys* 44: 303–312. https://doi.org/10.1016/S0926-9851(00)00008-2
11. Borovsky JE, Shprits YY (2017) Is the *Dst* index sufficient to define all geospace storms? *J Geophys Res Space Phys* 122: 11543–11547. https://doi.org/10.1002/2017JA024679
12. Borovsky JE, Denton MH (2006) The differences between CME-driven storms and CIR-driven storms. *J Geophys Res* 111: A07S08. https://doi.org/10.1029/2005JA011447
13. McPherron RL, Weygand J (2006) The solar wind and geomagnetic activity as a function of time relative to corotating interaction regions. In: Tsurutani B, McPherron R, Lu G, et al. Eds., *Recurrent Magnetic Storms*, Washington, DC: American Geophysical Union, 125–137. https://doi.org/10.1029/167GM12
14. Oghli HM, Akhbari M, Kalaki A, et al. (2020) Design and analysis of the cathodic protection system of oil and gas pipelines, using distributed equivalent circuit model. *J Nat Gas Sci Eng* 84: 103701. https://doi.org/10.1016/j.jngse.2020.103701
15. Yu Z, Hao J, Liu L, et al. (2019) Monitoring Experiment of Electromagnetic Interference Effects Caused by Geomagnetic Storms on Buried Pipelines in China. *IEEE Access* 7: 14603–14610. https://doi.org/10.1109/ACCESS.2019.2893963
16. Moraes JF, Paulino I, Alves LR, et al. (2020) Evaluation of possible corrosion enhancement due to telluric currents: case study of the Bolivia–Brazil pipeline. *Ann Geophys* 38: 881–888. https://doi.org/10.5194/angeo-38-881-2020
17. Larocca PA, Arecco MA, Macrino AC (2021) Anomalous geoelectric potential variations observed along a gas pipeline section in Argentine, possible intensification with variations of the Earth's magnetic field. *Earth Sci Res J* 25: 363–369. https://doi.org/10.15446/esrj.v25n4.91059
18. Larocca P, Arecco MA, Barredo SP (2022) Posible riesgo de corrosión en gasoductos enterrados en suelos resistivos por variaciones del potencial caño-suelo anómalos. En el 11th Congreso de Exploración y desarrollo de hidrocarburos (CONEXPLO22), Realizado del 8 al 11 de noviembre, Mendoza, Argentina. 473–481. Available from: https://www.iapg.org.ar/conexplo/PENDRIVE/pdf/sesiones-generales/geofisica/geofisica25.pdf.
19. Pereyra FX, Fratalocchi CN, Tchilinguirian P, et al. (2001) Carta de Línea de Base Ambiental 3763–IV-Coronel Suárez Provincia de Buenos Aires. Servicio Geológico Minero Argentino.
20. Pereyra FX (2012) Suelos de la Argentina. Geografía de suelos, factores y procesos formadores. *Buenos Aires, Argentina: Editorial SEGEMAR-AACS-GAEA*. https://repositorio.segemar.gov.ar/handle/308849217/3619.

21. Morari F, Castrignanò A, Pagliarin C (2009) Application of multivariate geostatistics in delineating management zones within a gravelly vineyard using geo-electrical sensors. *Comput Electron Agric* 68: 97–107. https://doi.org/10.1016/j.compag.2009.05.003
22. Rostoker G, Friedrich E, Dobbs M (1997) Physics of magnetic storms. *Magnetic storms* 98: 149–160. https://doi.org/10.1029/GM098p0149
23. Loewe CA, Prölss GW (1997) Classification and mean behavior of magnetic storms. *J Geophys Res Space Phys* 102: 14209–14213. https://doi.org/10.1029/96JA04020
24. Matzka J, Stolle C, Yamazaki Y, et al. (2021) The geomagnetic Kp index and derived indices of geomagnetic activity. *Space Weather* 19. https://doi.org/10.1029/2020SW002641
25. Tapping K (2013) The 10.7 cm solar radio flux ($F_{10.7}$). *Space Weather* 11: 394–406. https://doi.org/10.1002/swe.20064
26. Blakely R (1996) *Potential theory in gravity and magnetic applications*. Cambridge University Press, London, 461.
27. Cooper GRJ, Cowan DR (2006) Enhancing potential field data using filters based on the local phase. *Comput Geosci* 32: 1585–1591. http://dx.doi.org/10.1016/j.cageo.2006.02.016
28. Shore RM, Freeman MP, Wild JA, et al. (2017) A high-resolution model of the extemal and induced magnetic field at the Earth's surface in the Northem Hemisphere. *J Geophys Res Space Phys* 122: 2440–2454. https://doi.org/10.1002/2016JA023682
29. Conde D, Castillo FL, Escobar C, et al. (2023) Forecasting geomagnetic storm disturbances and their uncertainties using deep learning. *Space Weather* 21: e2023SW003474. https://doi.org/10.1029/2023SW003474
30. Opgenoorth HJ, Robinson R, Ngwira CM, et al. (2024) Earth's geomagnetic environment-progress and gaps in understanding, prediction, and impacts. *Adv Space Res*. In Press. https://doi.org/10.1016/j.asr.2024.05.016
31. Soil Survey Staff, Keys to Soil Taxonomy. 11th Edition, USDA-NRCS, Washington DC, 2010. 338. Available from: https://nrcspad.sc.egov.usda.gov/DistributionCenter/product.aspx?ProductID=837.
32. Panigatti JL (2010) Argentina 200 años, 200 suelos. Buenos Aires: Ediciones INTA. Available from: https://www.academia.edu/40540943/ARGENTINA_200_A%C3%91OS_200_SUELOS.